SCIENTIFIC REPORTS

OPEN

SUBJECT AREAS:
ELECTRONIC DEVICES
NANOPARTICLES
NANOSENSORS
ELECTRONIC MATERIALS

Received
11 April 2013

Accepted
19 August 2013

Published
10 September 2013

Correspondence and requests for materials should be addressed to Y.-G.G. (ygguo@iccas.ac.cn) or L.-J.W. (wanlijun@iccas.ac.cn)

Integrated Prototype Nanodevices via SnO_2 Nanoparticles Decorated SnSe Nanosheets

Jian-Jun Wang[1,3], Ai-Feng Lv[2,3], Yong-Qing Wang[1,3], Bo Cui[1,3], Hui-Juan Yan[1,3], Jin-Song Hu[1,3], Wen-Ping Hu[2,3], Yu-Guo Guo[1,3] & Li-Jun Wan[1,3]

[1]Key Laboratory of Molecular Nanostructure and Nanotechnology, Institute of Chemistry, Chinese Academy of Sciences, Beijing 100190, China, [2]Key Laboratory of Organic Solids, Institute of Chemistry, Chinese Academy of Sciences, Beijing 100190, China, [3]Beijing National Laboratory for Molecular Sciences, Beijing 100190, China.

Hybrid materials made from all inorganic components are intriguing in many fields, because they have shown in-depth potential use for electronic and optoelectronic applications including solar cells, gas sensors, photodetectors, and field effect transistors. Hybrid materials made from SnO_2 nanoparticles on SnSe nanosheets have been synthesized via a facile, lost-cost and safe solution method, and have been demonstrated as promising multifunctional materials in various prototype devices, including gas sensors, photodetectors, and field effect transistors.

Recent technological breakthroughs and the desire for new functions generate an enormous demand for novel materials. Many of the well-established materials, such as metals, semiconductors, cannot fulfil all technological desires for the various new applications. Hybrid nanomaterials have been significantly investigated in fundamental and industrial laboratories, because they either show characteristics between the two original phases or even new properties[1–3]. On the other hand, nowadays, electronic circuits becoming smaller and smaller from laboratories to fabrication facilities[4–6]. The development of nanomaterials and the increasing demand for miniaturization and integration of devices all point to the cross-disciplinary role of multifunctional nanostructure[7–9]. Therefore, developing and synthesizing multifunctional nanoscale materials are needed to construct multifunctional devices and understand the design rules for next generation of electronic circuits. Here, we report that integrated prototype nanodevices via SnO_2 nanoparticles decorated SnSe nanosheets, which have shown applications in gas sensing, photodetector, and field effect transistor.

Results

Recently, Sn-based materials including SnSe and SnO_2, as low-cost and eco-friendly materials with capability of bandgap engineering, have driven considerable attention[10–20]. Colloidal nanocrystals (NCs) have been considerably investigated and demonstrated the promising applications due to their low cost and easily scalable production, as well as unique chemical and physical properties[21–24]. Hybrid materials made from SnO_2 nanoparticles on SnSe nanosheets have been synthesized via a facile, lost-cost and safe solution method. The structure of the as-synthesized products was characterized by X-ray diffraction (XRD), as shown in Figure 1. The powder X-ray diffraction (XRD) pattern of the as-prepared products (Figure 1a) can be indexed to the orthorhombic SnSe structure (JCPDS no. 65-6459), with no additional crystalline impurity phases evident. It's found that no peaks of SnO_2 phase was observed, which may be due to the low content, low crystalline, or small size of SnO_2 in the hybrid materials. It's also noteworthy that a strong (400) diffraction peak is observed for the NCs relative to standard pattern, which indicates the as-prepared SnSe nanosheets have (400) textured structure.

X-ray photoelectron spectroscopy (XPS) analysis was used to confirm the oxidation states of the three elements, indicating that all the elements are in the oxidation states as expected in SnO_2/SnSe nanosheets (Figure 1b and Figure S2). Especially, the Sn $3d_{5/2}$ and $3d_{3/2}$ peaks have been split into two peaks, respectively, due to the two different chemical states of Sn. The Sn3d band obtained from the XPS analysis (Figure 1b) can well be fitted into two components. The peaks of 494.7 eV and 486.3 eV can be ascribed to the Sn $3d_{5/2}$ and $3d_{3/2}$ peak from SnO_2, and the peaks at 493.2 eV and 484.8 eV can be attributed to SnSe. Furthermore, the Sn/Se ratio measured with XPS analysis show an average ratio of 69.9 : 30.1, confirming the existence of SnO_2 nanoparticles.

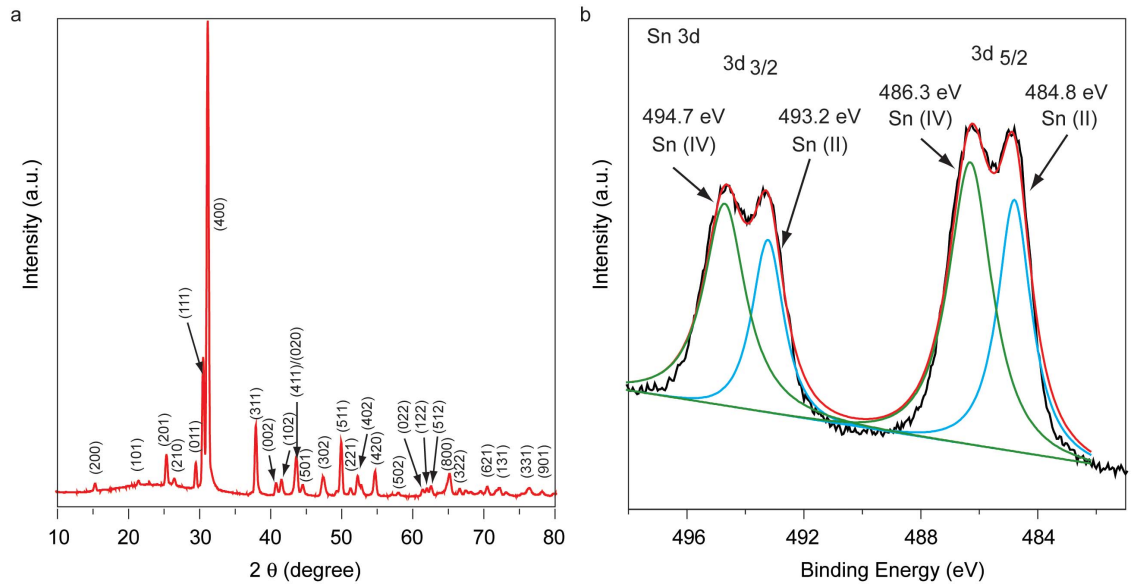

Figure 1 | Structure characterization. (a) A XRD pattern of as-synthesized sample. (b) High-resolution XPS spectrum of Sn 3d.

In order to confirm the morphology of the hybrid nanosheet, AFM was used to touch the nanosheet. As shown in Figure 2a and S1a, representative AFM images and the corresponding line scan profile provide an average nanosheet thickness ranging from 20 to 40 nm. Furthermore, the transparency of the nanosheets is also consistent with the previous report[18]. Figure 2b and S1b show HRAFM images of the surface of the hybrid nanosheet, demonstrating that the SnO_2 nanoparticles were homogenously distributed on the surface of SnSe

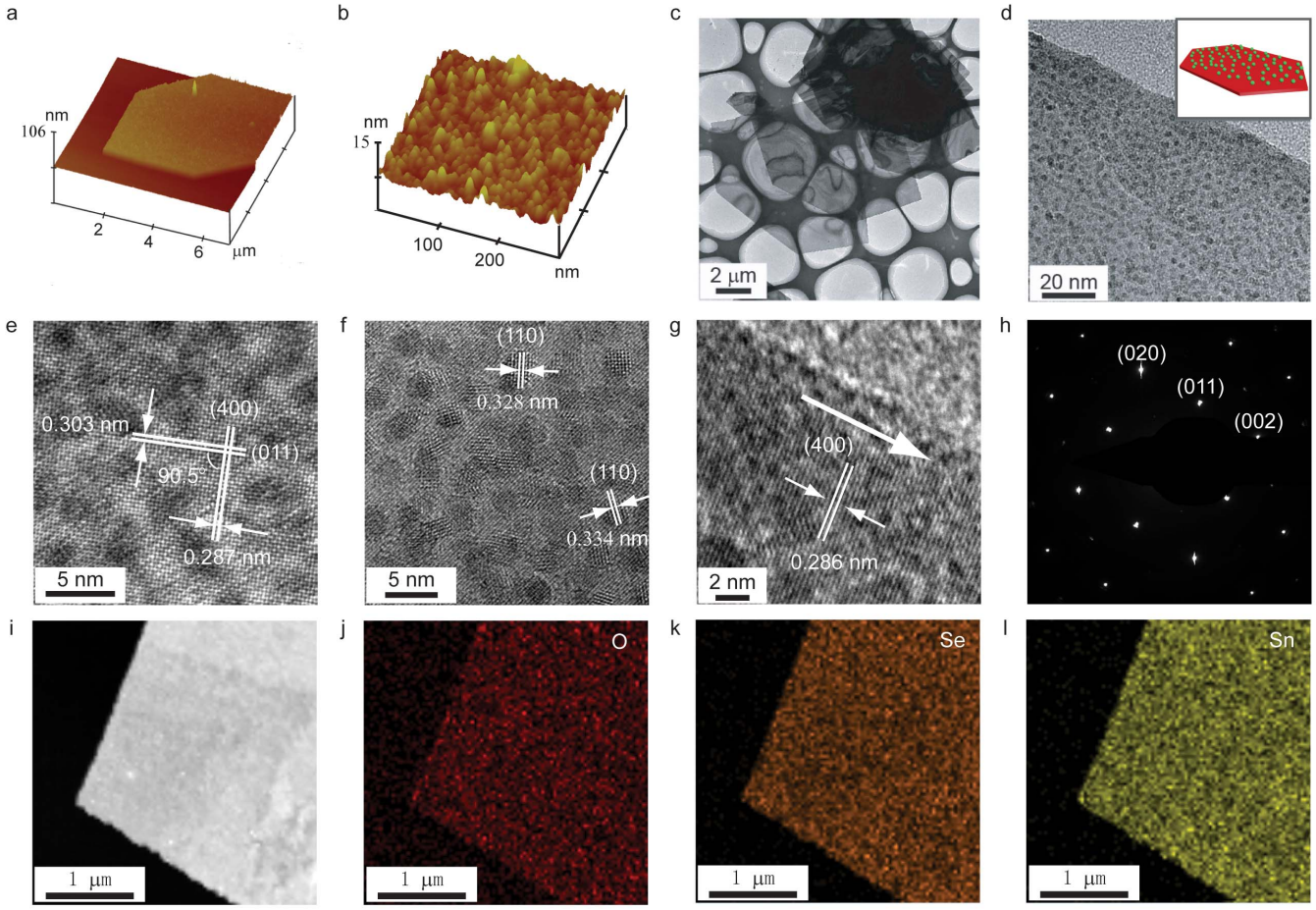

Figure 2 | Morphology and structure characterization of SnO_2/SnSe nanosheets. (a) the corresponding 3D AFM image. (b) HRAFM images of the surface of a SnO_2/SnSe nanosheet. (c, d) Low magnification TEM images, (e, f, g) HRTEM images, and (h) SAED patterns of a single nanosheet. STEM-EDS elemental maps of a single nanosheet. (i) STEM image, (j) O elemental map, (k) Se elemental map, (l) Sn elemental map.

nanosheets as shown in the inset of Figure 2d. The low resolution TEM image is shown in Figure 2c, indicating that the nanosheets have a hexagonal shape and the average smallest-edge length is range from 4 to 7 μm and the average largest-edge length is longer than 10 μm. Figure 2d shows a representative HRTEM image of a SnSe nanosheet. It is obvious to see that there are quantities of nanoparticles well-dispersed attaching to the nanosheet surface. From higher resolution TEM images (Figure 2e, f), it can be revealed that SnSe nanosheets show the monocrystalline nature with a lattice distance of 0.303 nm and 0.287 nm, well-matched to the (011) plane and (400) of orthorhombic SnSe. Furthermore, the two planes meet at an angle of 90.5° that is well in agreement with the theory value. As expected, the small particles attaching on the surface of SnSe nanosheets have an average diameter of 2 ~ 3 nm and the observed lattice distance of ~0.33 nm corresponds to the (110) plane of the tetragonal phase SnO_2 (JCPDS no. 41-1445). The small grain size of the obtained SnO_2 nanoparticles contributes to no SnO_2 peaks observed in the XRD pattern. The HRTEM image (Figure 2g) indicates that the growth direction of the SnSe nanosheets is oriented along the [100] lattice plane, as observed in the previous report on nanowires[14]. The electron diffraction pattern taken from an individual nanosheet (Figure 2h) shows a spot pattern that is consistent with the XRD result, and the spots are well indexed to (020), (011), and (002) planes of orthorhombic SnSe, indicating monocrystalline nature of the SnSe nanosheets.

To identify the element distribution of the as-synthesized nanosheets, STEM-EDS elemental maps were recorded from a single nanosheet. The results shown in Figure 2i, j, k, l reveal that the three elements of O, Sn, and Se are distributed very homogeneously in nanosheets and exhibit no apparent element separation or aggregation, also indicating that the SnO_2 quantum dots are indeed isolated with near monodispersion. Additionally, the Sn/Se ratio measured from several nanosheets with energy dispersive X-ray spectroscopy (EDS) analysis show an average ratio of 52.5 : 47.5. This ratio is larger than that in SnSe crystals due to the presence of SnO_2, and at the same time, it also indicates that the content of SnO_2 is relatively low in the hybrid products. This ratio is smaller than that of XPS results, further indicating that SnO_2 nanoparticles are dispersed on the surface of SnSe nanosheets.

In order to study the electrical properties of SnO_2/SnSe, field effect transistors (FETs) based on a single SnO_2/SnSe nanosheet were fabricated by using a mask method[25]. The nanosheets were first dispersed on a SiO_2/Si substrate with a desired density. Then, a micrometer-sized wire was laminated over the nanosheet as a shield mask and Au was vacuum evaporated on the substrate with a thickness of 60 nm. Finally, a device was successfully made after the mask was removed with the mechanical tips (Figure 3a). All the devices were recorded with a Keithley 4200 SCS and a Micromanipulator 6150 probe station in a clean and shielded box at ambient conditions, and typical p-type field effect transistor behavior was obtained. Output and transfer characteristics are shown in Figure 3b, c. These characteristics are highly reproducible and quite stable.

Discussion

From the output curve shown in Figure 3b, it could be known that the FET based on a single SnO_2/SnSe nanosheet works in the linear regime when $V_{sd} = -5$ V, therefore, the field effect mobility is determined by using the equation of $\mu = L^*K/(W^*C_i^*V_{sd})$, where L and W is the length and width of the channel, C_i is the capacitance per unit area of the gate dielectric layer (SiO_2, 300 nm, $C_i = 9.6$ nF/cm^2), V_{sd} is the voltage between the source and drain electrodes, and K is the slope of the transfer curve (Figure 3c). The hole mobility of the nanosheets was calculated to be about 1.4 $cm^2V^{-1}s^{-1}$.

SnSe is an attractive semiconductor for its appropriate bandgap, large absorption coefficient, less toxic and more environmentally responsible alternative to related narrow bandgap nanoparticles that contain lead or cadmium and is of interest as a light absorption layer for solar cells, photodetectors and near-infrared optoelectronic devices[14,15,18]. Upon illumination with photon energy larger than its bandgap (1.3 eV), the conductivity of a semiconductor would increase drastically due to the photoexcited electron–hole pairs. As expected, the nanosheets show a large absorption and a bandgap that overlaps well with the whole solar spectrum (Figure S4). In addition, the small SnO_2 quantum dots dispersed on the surface of SnSe nanosheets may decrease the mirror reflection of light, which contributes to the large absorption in the white light range. Figure 3d shows I–V curves measured in dark and during exposures to a white-light. The dark currents could approach more than 10 μA at a bias of 10 V, indicating the well crystalline of the nanosheets. With the light irradiation on and off, the currents past the nanosheet obviously increased at a light intensity of 5.6 mW cm^{-2} and a bias of 10 V, leading to a net increase of ~10.0 μA, which is much larger than varieties of chalcogenide single-crystalline based devices[26]. The current of the devices shows two distinct states, a "low" current state under dark conditions and "high" current state under light conditions (Figure 3e), and the switching in those two states was reversible and fast. This result indicates that the nanosheet can be used as a highly sensitive photodetectors. Interestingly, it has been found that, with a gate connection, it is obvious to note that, under light irradiation, our single-nanosheet transistors exhibited strong photodependence (Figure 3f), working as phototransistors. The currents of devices were controlled by the incident light and V_G. This suggests that the light and V_G could modulate the currents respectively and simultaneously, implying that the SnO_2/SnSe nanosheets based devices can be utilized as a new way to realize light detection and signal magnification for future low-cost, ultrahigh-density photoelectric integration.

Furthermore, SnO_2 has been demonstrated to be a good sensing material for harmful and toxic gases[10,16,20]. For our as-synthesized hybrid SnO_2/SnSe nanosheets, the gas sensitivity is expected because of the presence of small grain size SnO_2 with large surface-to-volume ratio dispersed on the surface of SnSe nanosheets. In our experiments, the gas sensitivity for carbon monoxide and ethanol was tested, respectively. It should be mentioned that the sensors show lower resistance than our other systems, which may be due to the high crystalline of the SnSe substrate. Figure S3a shows the on/off switching of the sensor when a thin-film made from nanosheets was exposed to carbon monoxide at a concentration of 500 ppm diluted in N_2 at 200°C. It was observed an obvious change in resistance between the on and off states. To simulate practical application, the response of sensors was studied in dry air. Figure 4a shows the responses of SnO_2/SnSe nanosheets to 100–1000 ppm CO diluted in dry air at 260°C. Initially, the sensor showed lower response at the low concentration (100 ppm). However, as the CO concentration increased, the sensor demonstrated larger response and the responses increase proportionally. Here it was found that the as-synthesized hybrid nanosheets exhibited both high sensitivity and reversibility. For ethanol sensing, the nanosheets also show high sensitivity as shown in Figure S3. A total change of nearly 3 times in resistance between the on and off states (Figure S3b) was observed at 260°C and a concentration of 500 ppm. The sensitivity is not as high as the reported value because of the low resistance and low content of SnO_2. The loading of SnO_2 can be estimated from Figure 2f. The fraction of SnO_2 coverage is 18.02% and the loading of SnO_2, $M_{SnO2}/(M_{SnSe} + M_{SnO2})$ is 1.70% (The details can be seen in supporting information). It is believed that the sensitivity could be increased by loading more SnO_2. In order to confirm the gas sensing properties and develop the application of a single nanosheet in gas sensing, the devices based on a single nanosheet were investigated. Figure 4b show the on/off switching of the sensor response to 1000 ppm CO diluted in dry air at room temperature, indicating the intrinsic gas sensing properties. Compared to the film sensors,

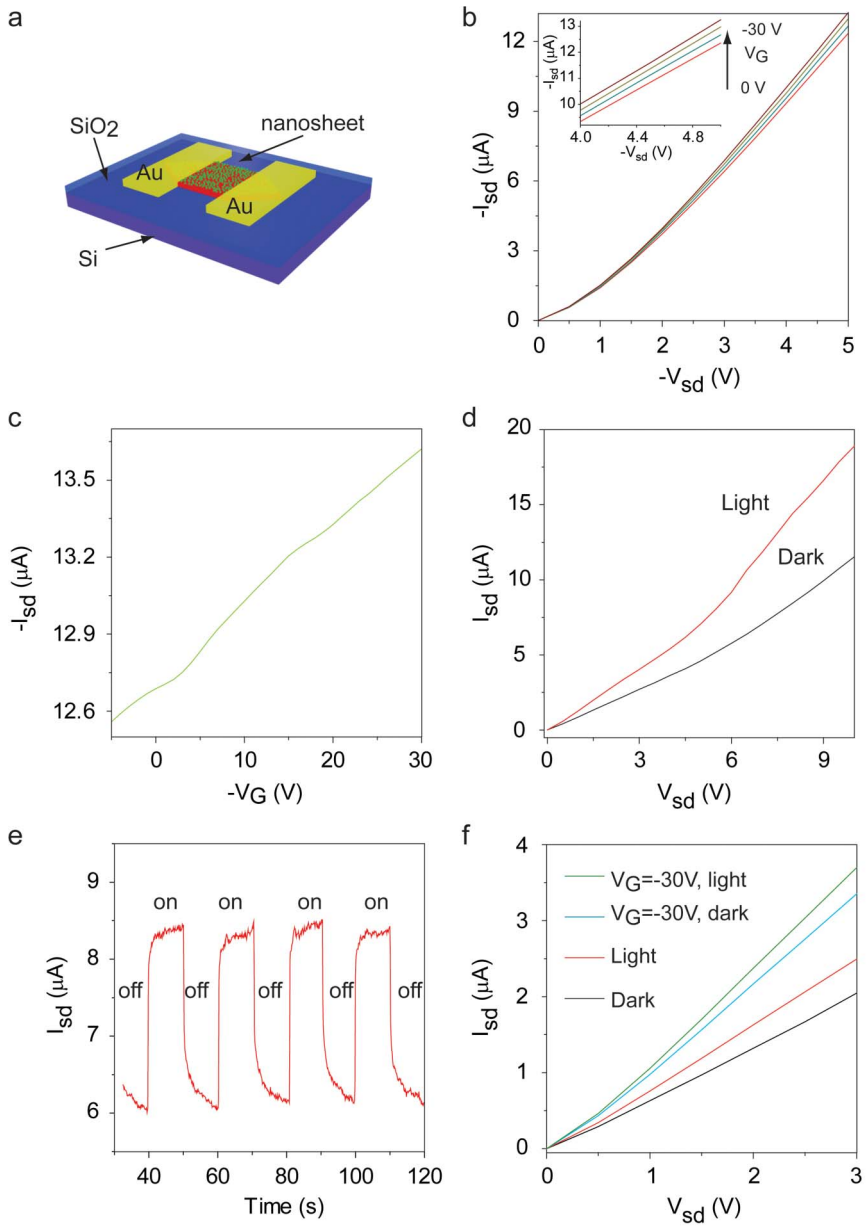

Figure 3 | Field effect transistors and photodetectors based on a single SnO_2/SnSe nanosheet. (a) Schematic structure of the device, (b) Output characteristics of the individual nanosheet transistors; (c) transfer characteristics of the device at a fixed source/drain voltage, $V_{SD} = -5$ V. (d) Dark current and photocurrents at an incident light densities of 5.6 mW cm^{-2}. (e) On/off switching of the device at an incident light density of 5.6 mW cm^{-2} and a bias voltage of 5 V. (f) different currents of the device without and with a gate voltage of −30 V in dark and under light.

the single nanosheet sensor could display obvious change of the conductivity even at room temperature and, furthermore, the short response time, which may be due to the good charge transport within the individual nanosheet. For the present sensors, it is believed that the high sensitivity and reversibility at low temperature can be attributed to the intrinsically small grain size (2 ~ 3 nm) and high surface-to-volume ratios of SnO_2 quantum dots. Furthermore, they are dispersed uniformly on the surface of SnSe nanosheets, generating larger area for absorbing gas, and the operation of such sensors also helps to eliminate grain size changes that might occur as a result of thermal-induced sintering.

The significance of our results is a demonstration that the multifunctional nanodevices can be fabricated by designing multifunctional nanostructures. SnSe can act as an effective light absorptive material, and at the same time, the small SnO_2 nanoparticle dispersed on the surface of SnSe nanosheets may decrease the mirror reflection of light, which contributes to the large absorption in the white light range. The hybrid nanostructure of SnO_2 quantum dots on SnSe nanosheets allows for a large density of SnO_2 quantum dots and eliminating grain size change during the thermal-induced sintering. The strategy is simple, yet very effective and of great perspective because of its versatility, it can also be extended to other optoelectronic functional materials for new phenomenon and functions.

Methods

Synthesis of hybrid SnO_2/SnSe nanosheets. The hybrid SnO_2/SnSe nanosheets were prepared via a facile solution method. In a typical synthesis, first, 1 mmol $Sn(Ac)_4$ was dissolved in 10 ml oleic acid and exchanged the ligands for 11 h at 150°C under Ar gas flow. The finall solution was marked as Sn source solution. Then 0.5 ml Sn source solution, 1 ml oleic acid, 6 ml oleylamine and 0.125 mmol diphenyl diselenide were added in a two neck flask. The mixture was heated to 240°C to react for 1 h after degassing. The products were washed three times by the mixture of toluene and ethanol. The final products were dispersed in ethanol for further characterization.

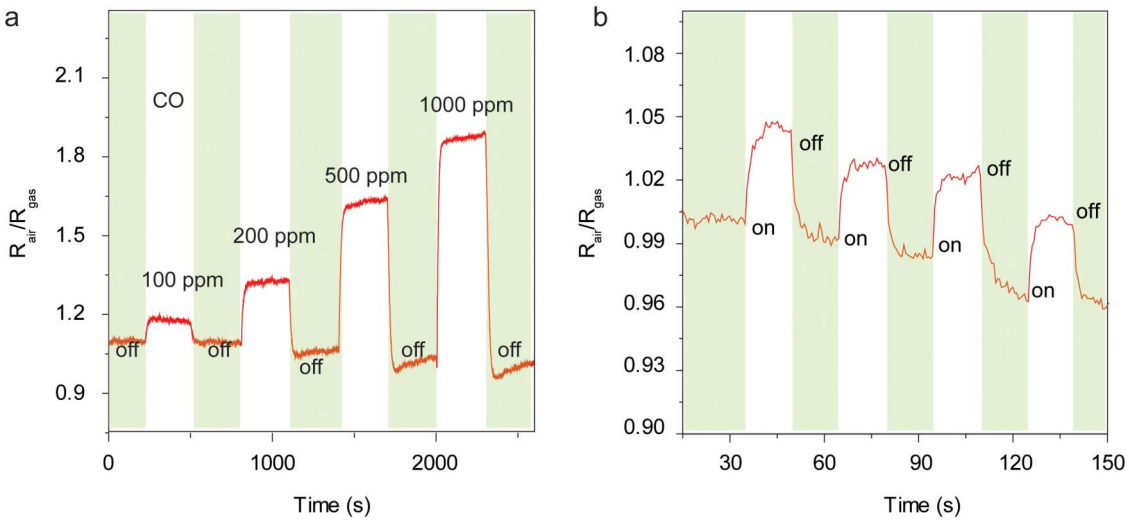

Figure 4 | Gas sensors based on SnO_2/SnSe nanosheets. (a) Transient response of the sensor to CO (100–1000 ppm) at 260°C. (b) on/off switching of the sensor response to 1000 ppm CO diluted in dry air at room temperature.

Characterization. The size and morphology of the NCs and high resolution transmission electron microscopy (HRTEM) images were characterized by using Tecnai G2 20S-TWIN and Tecnai G2 F20 X-Twin microscope working at an accelerating voltage of 200 kV. The phase and the crystallographic structure of the NCs were characterized by powder X-ray diffraction (PXRD) using a Regaku D/Max-2500 diffractometer equipped with a Cu Kα1 radiation (λ = 1.54056 Å). The composition of the as-synthesized NCs was analyzed by energy dispersive X-ray spectrometry (EDX) using a GENESIS system (EDAX Inc.) attached to the TEM. X-ray photoelectron spectroscopy data were obtained with an ESCALab220i-XL electron spectrometer from VG Scientific using 300 W AlKα radiation. The gas-sensing experiments were performed on a homemade sensor system. The sensor materials were dispersed in ethanol or water and dropped on a UST sensor device. The gas flow concentration was 200 sscm using a mass flow controller.

1. Mokari, T., Rothenberg, E., Popov, I., Costi, R. & Banin, U. Selective growth of metal tips onto semiconductor quantum rods and tetrapods. *Science* **304**, 1787–1790 (2004).
2. Cozzoli, P. D., Pellegrino, T. & Manna, L. Synthesis, properties and perspectives of hybrid nanocrystal structures. *Chem. Soc. Rev.* **35**, 1195–1208 (2006).
3. Wang, J.-J., Wang, Y.-Q., Cao, F.-F., Guo, Y.-G. & Wan, L.-J. Synthesis of Monodispersed Wurtzite Structure $CuInSe_2$ Nanocrystals and Their Application in High-Performance Organic-norganic Hybrid Photodetectors. *J. Am. Chem. Soc.* **132**, 12218–12221 (2010).
4. Tang, J., Huo, Z., Brittman, S., Gao, H. & Yang, P. Solution-processed core-shell nanowires for efficient photovoltaic cells. *Nature nanotech* **6**, 568–572 (2011).
5. Tian, B. *et al.* Coaxial silicon nanowires as solar cells and nanoelectronic power sources. *Nature* **449**, 885–889 (2007).
6. Jie, J. *et al.* Photoconductive characteristics of single-crystal CdS nanoribbons. *Nano Lett.* **6**, 1887–1892 (2006).
7. Zhang, M. *et al.* Strong, transparent, multifunctional, carbon nanotube sheets. *Science* **309**, 1215–1219 (2005).
8. Javey, A., Nam, S. W., Friedman, R. S., Yan, H. & Lieber, C. M. Layer-by-layer assembly of nanowires for three-dimensional, multifunctional electronics. *Nano Lett.* **7**, 773–777 (2007).
9. Liong, M. *et al.* Multifunctional inorganic nanoparticles for imaging, targeting, and drug delivery. *ACS nano* **2**, 889–896 (2008).
10. Han, X. *et al.* Synthesis of Tin Dioxide Octahedral Nanoparticles with Exposed High-Energy {221} Facets and Enhanced Gas-Sensing Properties. *Angew. Chem. Int. Ed.* **48**, 9180–9183 (2009).
11. Hickey, S. G., Waurisch, C., Rellinghaus, B. & Eychmuller, A. Size and Shape Control of Colloidally Synthesized IV-VI Nanoparticulate Tin(II) Sulfide. *J. Am. Chem. Soc.* **130**, 14978–14980 (2008).
12. Baumgardner, W. J., Choi, J. J., Lim, Y. F. & Hanrath, T. SnSe Nanocrystals: Synthesis, Structure, Optical Properties, and Surface Chemistry. *J. Am. Chem. Soc.* **132**, 9519–9521 (2010).
13. Kovalenko, M. V. *et al.* SnTe nanocrystals: A new example of narrow-gap semiconductor quantum dots. *J. Am. Chem. Soc.* **129**, 11354–11355 (2007).
14. Liu, S. *et al.* Solution-Phase Synthesis and Characterization of Single-Crystalline SnSe Nanowires. *Angew. Chem. Int. Ed.* **50**, 12050–12053 (2011).
15. Franzman, M. A., Schlenker, C. W., Thompson, M. E. & Brutchey, R. L. Solution-Phase Synthesis of SnSe Nanocrystals for Use in Solar Cells. *J. Am. Chem. Soc.* **132**, 4060–4061 (2010).
16. Wang, Y. L., Jiang, X. C. & Xia, Y. N. A solution-phase, precursor route to polycrystalline SnO_2 nanowires that can be used for gas sensing under ambient conditions. *J. Am. Chem. Soc.* **125**, 16176–16177 (2003).
17. Xu, Y., Al-Salim, N., Bumby, C. W. & Tilley, R. D. Synthesis of SnS Quantum Dots. *J. Am. Chem. Soc.* **131**, 15990–15991 (2009).
18. Vaughn, D. D., In, S. I. & Schaak, R. E. A Precursor-Limited Nanoparticle Coalescence Pathway for Tuning the Thickness of Laterally-Uniform Colloidal Nanosheets: The Case of SnSe. *ACS Nano* **5**, 8852–8860 (2011).
19. Dattoli, E. N. *et al.* Fully Transparent Thin-Film Transistor Devices Based on SnO_2 Nanowires. *Nano Lett.* **7**, 2463–2469 (2007).
20. Park, M.-S. *et al.* Preparation and Electrochemical Properties of SnO_2 Nanowires for Application in Lithium-Ion Batteries. *Angew. Chem. Int. Ed.* **46**, 750–753 (2007).
21. Sukhovatkin, V., Hinds, S., Brzozowski, L. & Sargent, E. H. Colloidal quantum-dot photodetectors exploiting multiexciton generation. *Science* **324**, 1542–1544 (2009).
22. Wang, J. J., Hu, J. S., Guo, Y. G. & Wan, L. J. Wurtzite $Cu_2ZnSnSe_4$ nanocrystals for high-performance organic–inorganic hybrid photodetectors. *NPG Asia Materials* **4**, e2 (2012).
23. Gur, I., Fromer, N. A., Geier, M. L. & Alivisatos, A. P. Air-stable all-inorganic nanocrystal solar cells processed from solution. *Science* **310**, 462–465 (2005).
24. Lee, J. S., Kovalenko, M. V., Huang, J., Chung, D. S. & Talapin, D. V. Band-like transport, high electron mobility and high photoconductivity in all-inorganic nanocrystal arrays. *Nature Nanotech.* **6**, 348–352 (2011).
25. Jiang, L. *et al.* Organic Single-Crystalline Ribbons of a Rigid "H"-type Anthracene Derivative and High-Performance, Short-Channel Field-Effect Transistors of Individual Micro/Nanometer-Sized Ribbons Fabricated by an "Organic Ribbon Mask" Technique. *Adv. Mater.* **20**, 2735–2740 (2008).
26. Zhai, T. *et al.* Recent Developments in One-Dimensional Inorganic Nanostructures for Photodetectors. *Adv. Funct. Mater.* **20**, 4233–4248 (2010).

Acknowledgements

This work was supported by the National Natural Science Foundation of China (Grant Nos. 51225204, 21173237 and 91127044), the National Key Project on Basic Research (Grant Nos. 2012CB932900, 2011CB935700 and 2011CB932300), and the Chinese Academy of Sciences.

Author contributions

Y.G.G. and L.J.W. proposed and supervised the project; J.J.W., J.S.H., Y.G.G. and L.J.W. designed the experiments; J.J.W., A.F.L., Y.Q.W., B.C. and H.J.Y. synthesized the samples and did characterizations; J.J.W., J.S.H., W.P.H., Y.G.G. and L.J.W. analyzed data and wrote the manuscript, all authors participated in discussions of the results and in preparing the manuscript.

Additional information

Supplementary information accompanies this paper at http://www.nature.com/scientificreports

Competing financial interests: The authors declare no competing financial interests.

How to cite this article: Wang, J. *et al*. Integrated Prototype Nanodevices via SnO_2 Nanoparticles Decorated SnSe Nanosheets. *Sci. Rep.* **3**, 2613; DOI:10.1038/srep02613 (2013).